Massachusetts Institute of Technology

Theory of Water Desalination with Intercalation Materials

K. Singh,[1,2] H. J. M. Bouwmeester,[3] L. C. P. M. de Smet,[1,2] M. Z. Bazant,[4,5] and P. M. Biesheuvel[2]

[1]*Laboratory of Organic Chemistry, Wageningen University,*
Stippeneng 4, 6708 WE Wageningen, The Netherlands
[2]*Wetsus, European Centre of Excellence for Sustainable Water Technology,*
Oostergoweg 9, 8911 MA Leeuwarden, The Netherlands
[3]*Electrochemistry Research Group, Membrane Science and Technology,*
Department of Science and Technology, MESA$^+$ Institute for Nanotechnology, University of Twente,
Drienerlolaan 5, 7522 NB Enschede, The Netherlands
[4]*Department of Chemical Engineering, Massachusetts Institute of Technology,*
Cambridge, Massachusetts 02139, USA
[5]*Department of Mathematics, Massachusetts Institute of Technology,*
Cambridge, Massachusetts 02139, USA

We present a porous electrode theory for capacitive deionization with electrodes containing nanoparticles that consist of a redox-active intercalation material. A geometry of a desalination cell is considered which consists of two porous electrodes, two flow channels, and an anion-exchange membrane, and we use the Nernst-Planck theory to describe ion transport in the aqueous phase in all these layers. A single-salt solution is considered, with unequal diffusion coefficients for anions and cations. Similar to previous models for capacitive deionization and electrodialysis, we solve the dynamic two-dimensional equations by assuming that the flow of water, and thus the advection of ions, is zero in the electrode, and in the flow channel only occurs in the direction along the electrode and membrane. In all layers, diffusion and migration are only considered in the direction perpendicular to the flow of water. Electronic as well as ionic transport limitations within the nanoparticles are neglected, and instead the Frumkin isotherm (or regular solution model) is used to describe local chemical equilibrium of cations between the nanoparticles and the adjacent electrolyte, as a function of the electrode potential. Our model describes the dynamics of key parameters of the CDI process with intercalation electrodes, such as effluent salt concentration, the distribution of intercalated ions, cell voltage, and energy consumption.

I. INTRODUCTION

Capacitive deionization (CDI) is a method of water desalination where two porous electrodes adsorb ions from the aqueous phase, and later release the ions again [1–3]. Salt removal is achieved by alternatingly charging and discharging the electrodes which are connected through an electrical circuit. The porous electrodes typically contain three phases: water-filled pores for ion transport, a conducting material for electronic current, and a phase where ions are temporarily stored, see Fig. 1. Most work on CDI uses electrodes with ion storage in materials based on carbon (activated carbon, carbon nanotubes, graphene, etc.) where ions are stored in the electrical double layer (EDLs) along the carbon surface [4].

Another class of materials for ion storage is based on intercalation host compounds, which are examples of redox-active materials that are receiving increased attention because of their potential for higher salt adsorption, lower energy consumption, and tunable ion selectivity. Although our general theory below could be applied to arbitrary

intercalation compounds, adsorbing cations or anions, we will focus on the more common case of cation intercalation. Examples of such materials are nickel hexacyanoferrate (NiHCF), which is a Prussian blue analogue [5–11], sodium manganese oxide (NMO) [12–16], and iron or titanium phosphates [16,17] (which are also used in Li-ion batteries). In response to an applied voltage, cations intercalate, or are reversibly inserted, into the these redox-active host materials. The host crystal structure contains transition metal atoms, such as Fe or Mn which change redox state upon injection of electronic charge. When this material is charged more negatively (redox atoms in the crystal are reduced), to maintain electroneutrality extra cations are incorporated in the pores of the crystal, thus desalinating the water outside the particles. The intercalation materials mentioned above are highly cation selective (not incorporating anions), since the crystal is negatively charged, which provides a background countercharge for the intercalated cations.

To describe desalination by traditional CDI based on double-layer charging, porous electrode theory has been
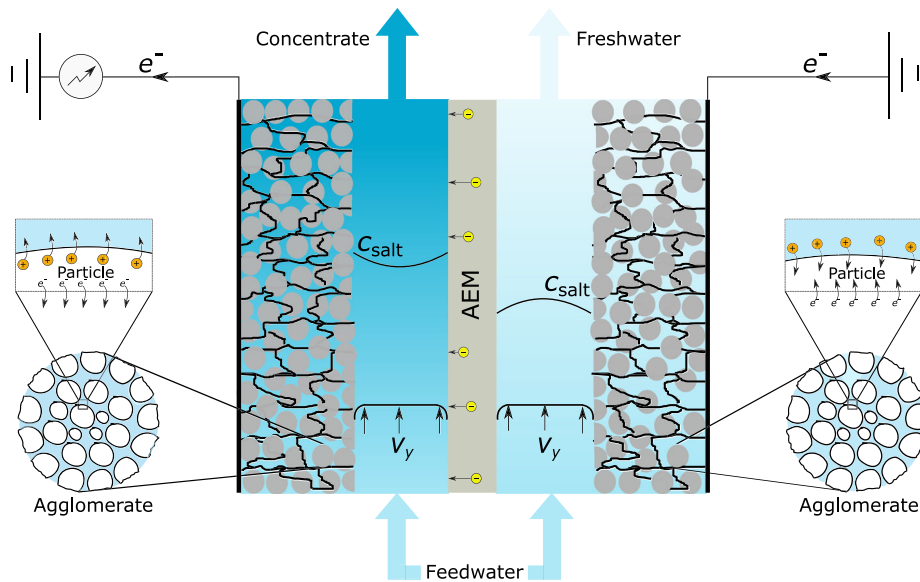
FIG. 1. Schematic of the CDI cell with porous electrodes containing nanoparticles of redox-active intercalation material. Electronic connections through the electrode (drawn as black lines) allow for the injection of charge from an external circuit. Nanoparticles are aggregated into water-filled agglomerates. The electrodes are separated by a pair of spacer channels for water flow, and an anion-exchange membrane which preferentially allows the transport of anions. The schematic captures the moment when ionic current flows left to right leading to deintercalation of Na^+ on the left, and intercalation on the right. Depicted in the spacer channels are typical profiles in salt concentration and velocity of the water.

used since the 1970s [18,19]. Johnson and Newman developed the first such theory for CDI and made the assumption that for each electron injected in the EDL of a carbon matrix, one counterion adsorbs [18]. Going beyond this approximation, Bazant *et al.* initiated the microscopic theory of double-layer charging dynamics and salt removal for the model problem of parallel-plate blocking electrodes [20]. Since 2010, Biesheuvel and Bazant incorporated this physics into a porous electrode theory for double-layer CDI, applied to carbon-based materials [21], which allows for incorporation of any quasiequilibrium, thin or thick, EDL structure. This generalized theory can be used for EDL models that consider both counterions and co-ions, ion mixtures of arbitrary valency, the presence of chemical surface charge, and Faradaic charge transfer [22].

Porous electrode theories have also been developed for intercalation materials, albeit motivated by applications to Li-ion batteries rather than CDI. In 1982, West *et al.* [23] presented a porous electrode theory for energy storage in intercalation, or insertion, materials, where the Nernst-Planck theory describes both ion transport across the porous electrode and inside the intercalation material. At the interface of electrolyte and intercalation material, the Frumkin intercalation isotherm is used [24,25], which provides a relation between electrode potential (relative to the electrolyte phase), ion concentration in solution, and the intercalation degree (the degree to which the intercalation material is filled with cations). This isotherm is an example of more general regular solution theory describing the homogeneous Gibbs free energy of mixing of two or more constituents with finite size (e.g., mean-field approximation on a crystal lattice), as used in phase-field models of intercalation materials [26–28]. Regular solution models can be used to describe the thermodynamics of host materials containing multiple mobile ionic species and point defects, such as vacancies and interstitials, and form the basis for simulations

of nonlinear diffusion, phase separation, and electrochemical reactions [27], in both single-crystal nanoparticles and multiphase porous electrodes [19,29].

In the present work we set up and solve a model for CDI with intercalation materials along the lines of Johnson and Newman [18] and West *et al.* [23]. We simplify the model of West *et al.* by neglecting transport limitation within the intercalation material, a common approximation in the modeling of battery electrodes consisting of intercalation nanoparticles [29,30]. This is a valid assumption when the nanoparticles are very small and accessible on all sides by the ions in the electrolyte (water) with fast insertion reactions [19]. A rigorous criterion is not available for validity of this assumption in all situations, because ion transport in the electrode and adsorption in the particles is not a simple steady-state resistances-in-series process. But a first comparison can be made on the basis of a "critical flux" of Na^+ ions in the two phases, $J_{crit} = cD/L$, with c a typical concentration, D a typical diffusion coefficient, and L a typical distance. For the electrolyte we have $c = 10$ mM, $D = 2.2 \times 10^{-10}$ m^2/s (based on a porosity of 30% and tortuosity based on the Bruggeman equation), and $L = 250$ μm, while for the nanoparticles, $c = 2.2M$ (at $\vartheta = 0.5$ for NiHCF, see Ref. [8]), $D = 6.9 \times 10^{-16}$ m^2/s [31], and $L = 5$ nm (based on a particle with a size of 30 nm; note that for a sphere, a typical diffusion depth is equal to the volume-area ratio, which is one sixth of the size of the sphere). These numbers give a critical flux for Na^+ in the nanoparticles that is about 35× larger than in the electrolyte phase in the electrode, thus underpinning the choice to focus on transport in the electrolyte.

Though we simplify the model by West *et al.* [23], we also extend their approach (which is for a single electrode) by considering a full electrochemical cell consisting of two electrodes, two flow channels (also called spacers or spacer channels), and an anion-exchange membrane (AEM).

The geometry is sketched in Fig. 1. This cell design was invented by Smith and Dmello [14] to solve the problem of how to desalinate water using two electrodes made of intercalation materials that both are only capable of adsorbing cations.

An interesting difference of our model with that of Johnson and Newman [18] is that we do not assume a constant capacitance, but instead implement the Frumkin intercalation isotherm, which for several intercalation materials has been shown to accurately describe chemical equilibrium between the electron-conducting phase, intercalation material, and electrolyte [24,25,27,29]. According to this equation, capacitance is high when the intercalation degree in the material is at an intermediate value ($\vartheta = 0.5$), while it drops dramatically when the material either is almost saturated with ions ($\vartheta \to 1$) or almost empty ($\vartheta \to 0$).

The electrode model is combined with electrodiffusion of ions in the two flow channels and in the AEM (see geometry depicted in Fig. 1). For ion transport in the pores of the electrode, and in the flow channel, we implement that the ions have a different diffusion coefficient. Besides, we include a full description of the AEM, allowing the passage of both cations and anions. Because the membrane has a large concentration of positive fixed charge, the flux of anions is much larger than of cations. We make calculations of complete charge-discharge cycles and show the development over time of key parameters such as cell voltage, effluent salinity, and the intercalation degree of the electrodes.

Note that our theory considers the intercalation particles to fill up homogeneously, without phase separation inside the solid phase. This phase separation is not occurring for NiHCF in aqueous electrolyte, but does happen for other systems, such as Li insertion in $FePO_4$-based electrodes in organic solvent, where Li-dense and Li-sparse regions coexist within the same material. Extensions to porous electrode theory that are required to include phase separation in the solid phase are introduced and reviewed in Refs. [19,27,29].

For an electrochemical cell based on porous electrodes containing nanoparticles of redox-active intercalation material, the kinetics of ion adsorption depends on various transport processes, and each must be included in a complete theory for the entire device. These processes include

(1) Diffusion and migration of ions through the electrolyte-filled pores of the electrode;

(2) Ion insertion (intercalation) into the redox-active material, and transport across these particles;

(3) Electronic charge transport across the electrode, from an external current source all the way down into each nanoparticle;

(4) Ion transport (advection, diffusion and migration) in a transport channel located outside the electrode; and

(5) Transfer of ions across the ion-exchange membrane. In the present work, transport by processes 1, 4, and 5 is addressed, while instead of addressing items 2 and 3 in detail, the transport resistance related to these processes is assumed to be infinitely low. Note that we do not consider a rate limitation in the intercalation step of ion transfer between the electrolyte and the intercalation material. In many situations, this ion-transfer reaction may not be rate limiting, though it can be included in future extensions of our model, using various models of electrochemical reaction kinetics [14,27,29,32].

Similar to Johnson and Newman [18] and West *et al.* [23], we make use of the Nernst-Planck (NP) equation for ion transport, an equation which is valid for a sufficiently dilute electrolyte, and which describes each ion in the same way. This approach is mathematically different from models developed for (Li-ion) batteries, which incorporate a solution-phase potential as the driving force for the transport of cations [33]. This potential combines the electrical potential in solution with a term dependent on Li^+ ion concentration. Also thermodynamic nonidealities, beyond the NP equation, are incorporated in such state-of-the-art battery models. Though these battery models were also successfully applied for CDI with intercalation materials [14,34], nevertheless, in the present work we follow Refs. [18,23] and make use of porous electrode theory based on the NP equation. Advantages of the NP approach are that it is mathematically easier to understand and implement, and in a later stage can be readily extended to ionic mixtures. Such modifications are not so straightforward to implement in the available codes for battery models [29]. For a dilute electrolyte, the NP equation is a valid approximation, because thermodynamic nonidealities of the aqueous phase are not very pronounced. Thus, we use the ideal NP equation for migration and diffusion of each ionic species in the different elements in the cell, extended with an advection term for the flow channel.

In summary, in the present work we aim to develop and present a mathematical model for water desalination by CDI using porous electrodes consisting of nanoparticles of intercalation material. Our approach is to use a theoretical framework which is not excessively complicated while it describes a large number of the physical and chemical processes that take place in CDI with intercalation materials. At a later stage, the present model can be extended in a straightforward manner to describe mixtures of salts, by using a generalized Frumkin intercalation isotherm for ionic mixtures [8,35]. Such an extension would be very difficult to make in the classical theoretical framework of modeling Li-ion batteries that use quasielectrostatic potentials and concentrated solution theory. In our present work we discuss two different modes of operation of the electrochemical cell and the influence thereof on key parameters relevant for understanding cell performance (e.g., salt concentration, intercalation degree, and cell voltage).

II. THEORY

We make a calculation for a complete CDI desalination cell which consists of two electrodes, two spacer channels, and an anion-exchange membrane (AEM) which is placed in the middle of the cell, see Fig. 1. This arrangement, with the electrodes connected to an external electronic circuit, forms the desalination system that we will describe. The feed streams enter the spacer channels on one side and leave on the other, in a direction longitudinal to membrane and electrode. The spacer channels are in contact with an electrode on one side and the AEM on the other. The channels are not completely open, but contain a porous layer with a certain porosity ε_s and tortuosity τ_s. Feedwater is used with a sufficiently low salt concentration for the assumptions of dilute solution theory to hold (activity coefficient, $\gamma \sim 1$) [19]. Ion transport in these channels is described by the NP equation, extended to include advective flow,

$$\boldsymbol{J}_i = c_i v - \frac{\varepsilon_s}{\tau_s} D_i (\nabla c_i - z_i c_i \nabla \phi), \qquad (1)$$

where $\boldsymbol{J}_i$ is the flux of ion i, v is fluid velocity, and c_i is ion concentration. We relate the tortuosity of the porous material to porosity with the Bruggeman equation, $\tau = 1/\sqrt{\varepsilon}$, as we will also do in the electrode. Furthermore, D_i is the ion diffusion coefficient in free solution, z_i the valency of the ion, and ϕ is the dimensionless electric potential. Dimensions of this potential can be restored by multiplication with the thermal voltage $V_T = RT/F = k_B T/e$.

Mass conservation describes the change of ion concentration with time at any position in these channels according to

$$\varepsilon_s \frac{\partial c_i}{\partial t} = -\nabla \cdot \boldsymbol{J}_i, \qquad (2)$$

which can be combined with Eq. (1) and further simplified by assuming that
(a) Water flow in the spacer channels only has a component in the y direction parallel to the membrane and electrode (see Fig. 1); hence, $v_x = 0$, and
(b) Diffusion and electromigration are only considered in the opposite, x, direction (which is perpendicular to the y direction of water flow).

With these assumptions, the balance for each ionic species in the spacer channel becomes [36]

$$\varepsilon_s \frac{\partial c_i}{\partial t} = -v_y \frac{\partial c_i}{\partial y} + \frac{\varepsilon_s}{\tau_s} D_i \left\{ \frac{\partial^2 c_i}{\partial x^2} + z_i \frac{\partial}{\partial x} \left(c_i \frac{\partial \phi}{\partial x} \right) \right\}, \qquad (3)$$

which is combined with local charge neutrality $\sum_i z_i c_i = 0$ and solved for each ionic species. For fluid velocity, we assume plug flow, thus v_y is independent of x.

The description of ion transport in the spacer channels acts as the basis for understanding the transport of ions in the porous electrodes, which results in the ion mass balance

$$\varepsilon_e \frac{\partial c_i}{\partial t} = \frac{\varepsilon_e}{\tau_e} D_i \left\{ \frac{\partial^2 c_i}{\partial x^2} + z_i \frac{\partial}{\partial x} \left(c_i \frac{\partial \phi}{\partial x} \right) \right\} - a J_{\text{int},i}, \qquad (4)$$

where ε_e is electrode porosity (volume fraction of electrode filled with electrolyte), and τ_e is electrode tortuosity. In the electrode the fluid velocity is set to zero. Similar to the spacer channel, electroneutrality is assumed in the electrolyte pore phase in the electrodes. In the model presented here, this corresponds to $[\text{Na}^+] = [\text{Cl}^-]$. The new addition in Eq. (4), $a J_{\text{int},i}$, is the ion flux from electrolyte into the intercalation material (redox-active nanoparticles), and is defined per unit area a, which is the area of the particles per unit volume of total electrode. For a perfectly cation-selective material, we have for all anions $J_{\text{int},i} = 0$, while for the cations, $J_{\text{int},i}$ follows from a balance over the nanoparticles. Assuming only a single cation to intercalate in the intercalation material, a cation mass balance for the nanoparticles is given by

$$c_{\max} \varepsilon_{\text{IM}} \frac{\partial \vartheta}{\partial t} = a J_{\text{int}}, \qquad (5)$$

where we leave out subscript i, and where $c_{\max}$ is the maximum possible concentration of cations in the intercalation material, ε_{IM} is the volume fraction of the intercalation material (as a fraction of the total electrode volume), and ϑ is the average cation intercalation degree (average fraction of active sites in the host particles occupied by a cation).

Finally, local chemical equilibrium is assumed between cations in the intercalation material and in the electrolyte. This chemical equilibrium is described using the Frumkin isotherm for intercalation [8,23,24]

$$\phi_{\text{ECM}} - \phi_\infty = \mu^\dagger - \ln \frac{\vartheta}{1 - \vartheta} + \ln \frac{c_+}{c_{\text{ref}}} - g(\vartheta - 1/2), \qquad (6)$$

where ϕ_{ECM} is the potential of the electron-conducting material (carbon in most cases), and ϕ is the potential in the nearby electrolyte phase, which is the same ϕ as used in Eq. (4). Furthermore, c_+ is the concentration of cations there, c_{ref} is a reference concentration, and $\mu^\dagger$ and g are constant factors dependent on the type of cation, where g can be considered as an intercation repulsion energy. For NiHCF, the Frumkin isotherm fits very well equilibrium data for electrode potential versus charge [8]. As noted above, the Frumkin isotherm is equivalent to the regular solution model for the Gibbs free energy of mixing of intercalated ions and vacancies, which has been successfully used in phase-field models of Li-ion batteries [26,27,29].

In the electron-conducting phase in the electrode, the electronic resistance is considered to be zero. This implies that the potential here, ϕ_{ECM}, does not vary with position. However, it is different for cathode and anode, and it

varies in time. Thus, the voltage as measured between anode and cathode, the cell voltage, is given by $V_{cell} = V_T(\phi_{ECM,A} - \phi_{ECM,C})$ where A and C refer to anode and cathode.

Finally, ion transport in the AEM separating the two halves of the cell must be described. As in the other regions, transport of ions in the AEM is described by the NP equation (1). Ion transport by advection is neglected in the membrane. Similar to the electrodes and the spacer channels, it is assumed that diffusion and migration occur only in the x direction across the membrane of thickness δ_m. Accumulation of mass is neglected in the membrane and as a consequence, in the membrane the flux of each ion remains invariant with position x. An equal diffusion coefficient D_m, in which the term ε/τ is included, is assumed for all ions in the membrane, and we define a transfer coefficient $k_m = D_m/\delta_m$. The membrane is furthermore defined by the fixed charge density ωX, which is a positive number for an AEM. A typical value for a commercial membrane is of the order of $X = 4M$. This is a fixed charge concentration per unit aqueous phase in the membrane. For a binary monovalent electrolyte, charge neutrality in the membrane is given by $c_{+,m} - c_{-,m} + \omega X = 0$ and a total ion concentration in the membrane is defined as $c_{T,m} = c_{+,m} + c_{-,m}$. The total ion flux is $J_{ions,m} = J_{+,m} + J_{-,m}$ and the charge flux (ion current density) is $J_{ch,m} = J_{+,m} - J_{-,m}$.

When the fixed charge density in the membrane is much higher than the salinity outside the membrane, the ion concentrations and the electrical potential ϕ can be assumed to be varying linearly with position inside the membrane [37]. As a consequence, the fluxes $J_{ions,m}$ and $J_{ch,m}$ become

$$J_{ions,m} = -k_m(\Delta c_{T,m} - \omega X \Delta \phi_m),$$
$$J_{ch,m} = -k_m \langle c_{T,m} \rangle \Delta \phi_m, \qquad (7)$$

where $\langle ... \rangle$ is an average between values at the extreme ends of the membrane, and Δ refers to a difference between these positions (with fluxes defined from left to right, Δ is defined as "right" minus "left"). The total ion concentration on each side of the membrane is related to the salt concentration just outside (i.e., in the spacer channel, at a position right next to the membrane) c^*, as

$$c_{T,m} = \sqrt{X^2 + (2c^*)^2}, \qquad (8)$$

while the Donnan potential (change in electrical potential) across each membrane edge is given by

$$\Delta \phi_D = \sinh^{-1}(\omega X / 2c^*). \qquad (9)$$

III. RESULTS AND DISCUSSION

The calculations for the CDI cell are set up for an electrolyte with a single cation Na^+ that can intercalate into redox-active nanoparticles under the influence of an applied electrical current. As a specific geometrical example of an electrochemical desalination cell, we consider CDI with porous electrodes containing intercalation particles where the electrode has the spacer channel on one side and the "current collector" on the other side. Here, electronic current is injected in the electrode. The spacer channels are positioned next to the AEM which is in the middle of the cell, as shown in Fig. 1. The electrolyte, a NaCl solution, flows through the spacer channel and both ions diffuse in and out of the electrodes, while Cl^- ions (and some Na^+ ions) also diffuse through the membrane. Note that also other designs are possible: in Ref. [14] a cell design was theoretically analyzed with the water flowing through the electrodes, and in Ref. [8] the spacer channel was located on the other side of the electrodes (on the outsides of the cell).

A. Numerical aspects

The CDI cell model for our geometry is solved numerically, based on the conservation equations (3)–(5). These equations are used for both ions, for spacer and electrode, along with the Frumkin isotherm (6) and the equations for the membrane. In the x direction (left-right direction in Fig. 1), discretization of the partial differential equations in each domain is done using a large number of nodes (>20 in each domain), but in y direction we use only use a single node and an implicit Euler scheme (backward Euler). Because of this choice it is as if in the flow direction each flow line is one (very thin) "stirred tank," an approach successfully applied for CDI in Ref. [38] and for electrodialysis in Ref. [39]. For the low desalination degrees as obtained in the present work, discretization in the y direction into more nodes, will not significantly change the results of the calculations. Note that in the case of "one node in the y direction," the geometry of how inlets and outlets of the two cell compartments are oriented relative to one another (e.g., co-current vs countercurrent) does not matter; this only starts to influence the calculation outcome with a higher discretization in the y direction. Another numerical aspect of our model is as follows: with more than one node in the y direction, constant current operation, where a certain current I is made to flow from anode to cathode, requires solving all equations on each node in the y direction simultaneously, because current I will not be evenly distributed over all y coordinates. However, when a boundary condition of constant cell voltage is used, then it is actually possible to solve each y node "sequentially," i.e., one after the other. Especially for steady-state operation in electrodialysis, this is particularly useful. Finally, note that because

we have neglected diffusion and migration in the y direction, we do not have to deal with various numerical complications at the inlet and outlet of the cell, such as ionic currents straying outside the cell, or the choice of correct boundary conditions in advection-diffusion problems, where the concentration decay in the y direction can propagate upward into feed tubes; see, e.g., Ref. [40].

For our calculations, parameters are based on experiments in Ref. [8], resulting in: $c_{salt,inflow} = 10$ mM, $\varepsilon_s = 1.00$, $\varepsilon_e = 0.30$, $\varepsilon_{IM} = 0.50$, $c_{max} = 4.4M$, cell area $A = 36$ cm^2, electrode thickness $\delta_e = 250$ μm, spacer thickness $\delta_s = 700$ μm, and water flow rate per channel $\Phi_v = 5.0$ mL/min, which results in a residence time of (water in) each spacer channel of $A\delta_s/\Phi_v = 30$ s. Diffusion coefficients of Na$^+$ and Cl$^-$ are 1.33×10^{-9} m^2/s and 2.00×10^{-9} m^2/s, respectively. For the membrane, the transfer coefficient is set to the value $k_m = 0.55$ μm/s (based on taking the average of D_{Na^+} and D_{Cl^-}, reducing that by a factor of 20, and implementing a membrane thickness of $\delta_m = 150$ μm). Membrane charge density is $X = 4.0M$ ($\omega = +1$ for an AEM). Operation is always with constant current at a value of $I = \pm 10$ mA. With this current running for one hour, this implies that the average intercalation degree in a certain electrode then changes by about $\Delta\vartheta = 0.20$, because $A\delta_e F \varepsilon_{IM} c_{max} \Delta\vartheta = I\Delta t$, where Δt is the time period of charging. For the intercation repulsion g, we use $g = 3.50$ (dimensionally, 90 mV). The factor $\mu^\dagger$ does not influence any calculation output and neither does the choice of c_{ref}.

B. Initial charging and discharge

In all cases we start the calculation with both electrodes charged half-way, i.e., $\vartheta = 0.5$, without gradients in ϑ across the electrode. Then we charge one electrode relative to the other for a period of 1 h, resulting in one electrode reaching an average $\vartheta_{avg} = 0.30$ and the other $\vartheta_{avg} = 0.70$. Then we discharge (i.e., reverse the direction of current) for the same duration of 1 h, after which each electrode is back to $\vartheta_{avg} = 0.50$. These are average values of ϑ, with the profiles in ϑ across each electrode as presented in Fig. 2(c) for different moments during the first hour of charging, and in Fig. 2(d) for various times during discharge. The salt concentration profiles during these periods are presented in Figs. 2(a) and 2(b). This initial cycle of charge and discharge is also shown as the first 2 h in Fig. 3, as well as the first 2 h in Fig. 4.

C. Two modes of operation
of charge-discharge cycles

After that time (from $t = 2$ h onward), two distinct operational modes are considered. In mode 1, at $t = 2$ h we again reverse the current direction and go back to the situation we had at $t = 1$ h, at least in terms of ϑ_{avg}. This cycle is then repeated with the current reversed every hour. Mode 1 is depicted in Figs. 3(a) and 3(c) and in Fig. 4. Instead, in mode 2, at $t = 2$ h, nothing is changed, and the current continues such that after another hour, at $t = 3$ h, we reach a situation that the values of ϑ_{avg} are now reversed
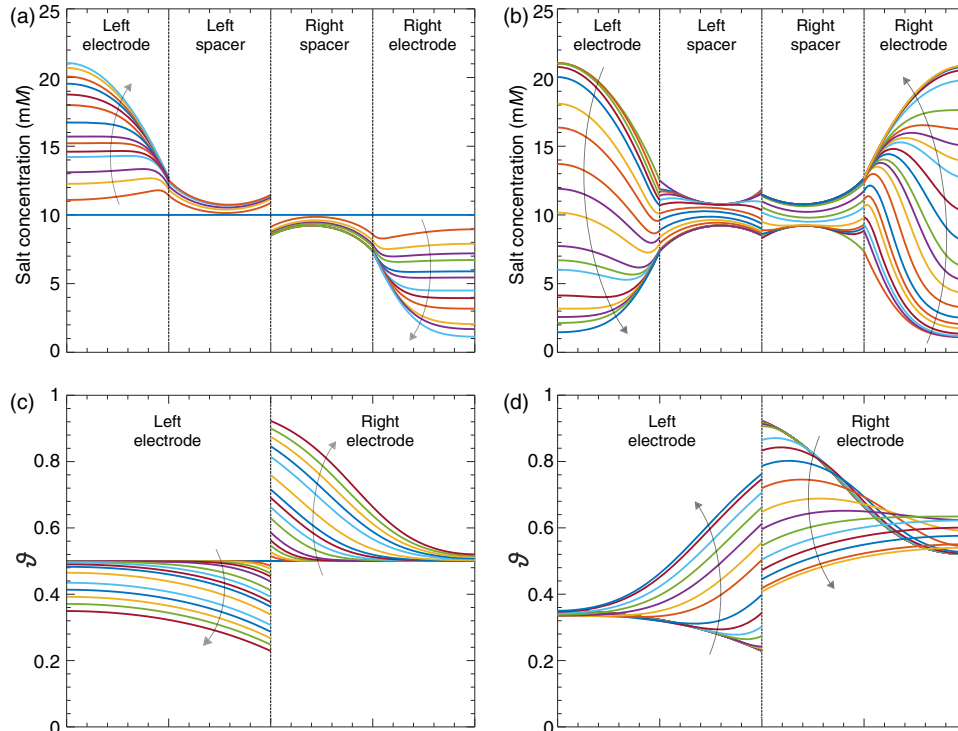

FIG. 2. Time-dependent profiles of salt concentration and intercalation degree during water desalination with intercalation electrodes. (a),(b) Salt concentration in electrodes and spacers; (c),(d) Intercalation degree in the two electrodes ϑ. These profiles are given as a function of position in the cell during (a),(c) first charging step, and (b),(d) first discharge step. Arrows depict the progression of time.
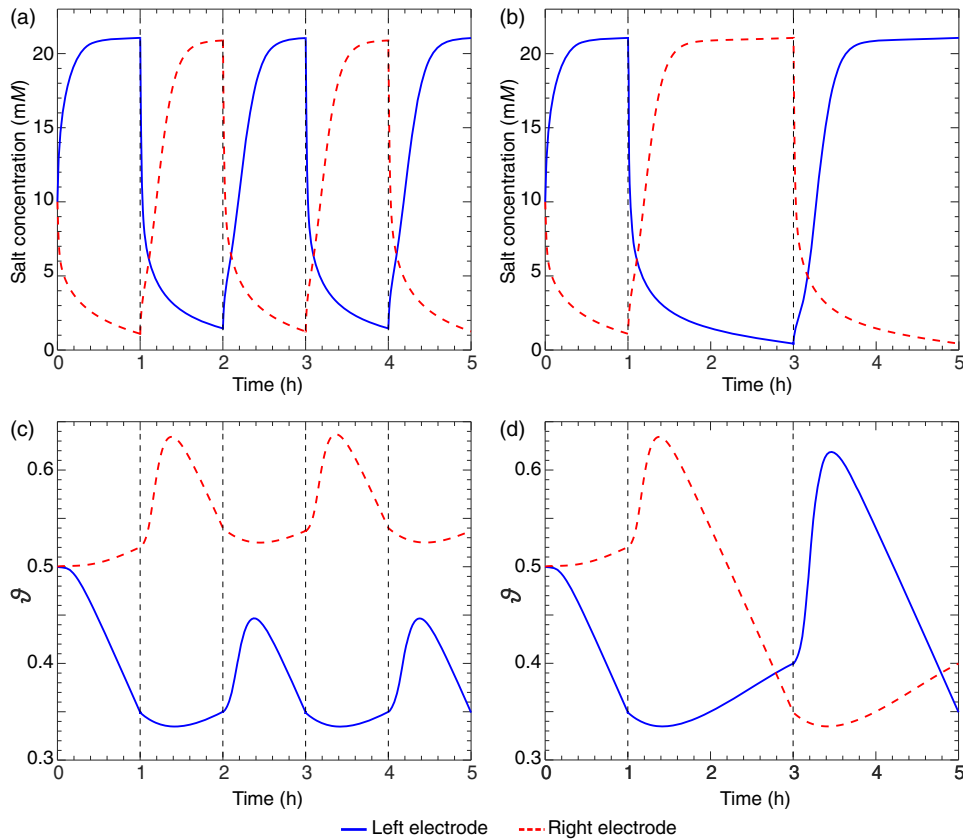
FIG. 3. Salt concentration and intercalation degree ϑ versus time for (a),(c) operation in mode 1, and (b),(d) operation in mode 2. In all cases calculation results are presented for the positions deepest in the electrode, thus farthest from the flow channel, for (a),(b) salt concentration, and (c),(d) intercalation degree.

compared to the situation at $t = 1$ h, i.e., the electrode that had $\vartheta_{avg} = 0.70$ at $t = 1$ h, now, at $t = 3$ h, has $\vartheta_{avg} = 0.30$ (and vice versa). Only now, at time $t = 3$ h, is the current reversed, and a period of charging starts that in 2 h will bring us back to the other end of the cycle (so that in terms of ϑ_{avg}, the cell is the same at $t = 5$ h as at $t = 1$ h). The main advantage of mode 2 operation is that (when the limit cycle is reached, and for a perfectly symmetric system) operation goes from a cell voltage of $+V$ at one end of the cycle, to a voltage of $-V$ at the other end, see Fig. 4. This symmetry is not found for operation according to mode 1. Thus, the mode 2 operation is very easily established experimentally by setting a value of $\pm V$ at which the cell reverses the direction of current.

Interestingly, in this mode 2 of operation where the current is reversed when the cell voltage is $\pm V$, each "half-cycle" is now exactly the same as that in the next half-cycle, with the only difference being that what happens in electrode 1 during a certain half-cycle, now happens in electrode 2 in the next. This can be observed in Fig. 3(d), where the red dashed line during period 1–3 h, is almost the same as the blue solid line in the period 3–5 h, and the same for the blue line in the period 1–3 h which can be compared with the red dashed line in the period 3–5 h. In Fig. 3, the behavior is not yet exactly the same because the limit cycle or "dynamic steady state" is not yet reached after 1 h. Interestingly, for operation in this mode 2, it is impossible to find an objective criterion about which half of the cycle is

to be called "charge" and which "discharge." There is no criterion because both halves of the cycle are exactly identical in terms of desalination performance, energy consumption, and other indicators. This exact symmetry occurs only when for both halves of the cell all operational settings are the same such as water flow rate and electrode mass. Interestingly, it is not necessary for both electrodes to have the same initial ϑ at time zero when we operate by fixing the end voltages of each step to $\pm V$.
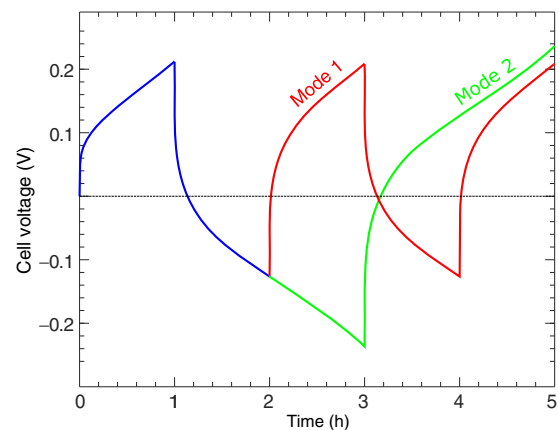

FIG. 4. Cell voltage for modes 1 and 2 of operation. The cell voltage changes suddenly when current changes direction. The blue curve shows the first cycle, while red and green refer to operation in modes 1 and 2, respectively.

Finally, we show in Fig. 4 calculation results for the development in time of cell voltage for the two modes of operation. These voltage-time (V-t) plots are important as they fully describe the electrical energy input in the process: for a constant current of $\pm I$, the electrical energy input is proportional to the area under the V-t curve (and delineated by the line $V_{\text{cell}} = 0$). As Fig. 4 shows, after reversal of the current direction, there is also a small "area" which corresponds to energy "output" (e.g., from 1 to 1.15 h), i.e., where energy recovery is in theory possible [41], after which a much longer period follows where energy must be invested to run the cell (from 1.15 to 3 h for mode 2).

IV. CONCLUSIONS

In conclusion, in this work we combine porous electrode theory for electrodes with redox-active intercalation materials with a description of spacer channels and a membrane, to describe an electrochemical system for capacitive deionization (CDI) with two intercalation electrodes that are chemically the same. The CDI cell design has an intrinsic symmetry as it is composed of two identical porous electrodes, both interfacing a spacer channel, separated by one anion-exchange membrane. We consider a single-salt solution, and calculated transport of ions by diffusion, migration, and advection in two directions. Transport of ions in the pores of the electrodes is modeled based on the Nernst-Planck equation. Thermodynamics of cation adsorption from electrolyte into the intercalation material is described by the Frumkin isotherm (regular solution theory), which factors in the lattice occupancy, intercation repulsion, electrolyte salinity and electrode potential. Homogeneous adsorption of ions is assumed, i.e., without phase separation within the nanoparticles. Including of this effect may be of importance for certain material chemistries. The required model extensions can be based on approaches discussed in Refs. [19,27,29].

In our model, a limitation in transport of ions within the intercalation material is neglected, just as is a resistance for flow of electronic current across the electrode. The model describes the development in time of salt concentration, intercalation degree, and cell voltage, parameters important for the description of performance of a CDI desalination cell. This work intends to provide a platform upon which future models can be constructed for more realistic water sources with ionic mixtures and for other geometries of desalination systems involving porous electrodes with redox-active intercalation materials.

ACKNOWLEDGMENTS

[1] M. E. Suss, S. Porada, X. Sun, P. M. Biesheuvel, J. Yoon, and V. Presser, Water desalination via capacitive deionization: What is it and what can we expect from it?, Energy Environ. Sci. **8,** 2296 (2015).

[2] P. M. Biesheuvel, M. Z. Bazant, R. D. Cusick, T. A. Hatton, K. B. Hatzell, M. C. Hatzell, P. Liang, S. Lin, S. Porada, J. G. Santiago, K. C. Smith, M. Stadermann, X. Su, X. Sun, T. D. Waite, A. van der Wal, J. Yoon, R. Zhao, L. Zou, and M. E. Suss, Capacitive deionization—Defining a class of desalination technologies, arXiv:1709.05925.

[3] F. He, P. M. Biesheuvel, M. Z. Bazant, and T. A. Hatton, Theory of water treatment by capacitive deionization with redox active porous electrodes, Water Res. **132,** 282 (2018).

[4] Z.-H. Huang, Z. Yang, F. Kang, and M. Inagaki, Carbon electrodes for capacitive deionization, J. Mater. Chem. A **5,** 470 (2017).

[5] K. Itaya, I. Uchida, and V. D. Neff, Electrochemistry of polynuclear transition metal cyanides: Prussian blue and its analogues, Acc. Chem. Res. **19,** 162 (1986).

[6] S. D. Rassat, J. H. Sukamto, R. J. Orth, M. A. Lilga, and R. T. Hallen, Development of an electrically switched ion exchange process for selective ion separations, Sep. Purif. Techn. **15,** 207 (1999).

[7] C. D. Wessells, S. V. Peddada, R. A. Huggins, and Y. Cui, Nickel hexacyanoferrate nanoparticle electrodes for aqueous sodium and potassium ion batteries, Nano Lett. **11,** 5421 (2011).

[8] S. Porada, A. Shrivastava, P. Bukowska, P. M. Biesheuvel, and K. C. Smith, Nickel hexacyanoferrate electrodes for continuous cation intercalation desalination of brackish water, Electrochim. Acta **255,** 369 (2017).

[9] T. Kim, C. A. Gorski, and B. E. Logan, Low energy desalination using battery electrode deionization, Environ. Sci. Technol. Lett. **4,** 444 (2017).

[10] F. Ma, Q. Li, T. Wang, H. Zhang, and G. Wu, Energy storage materials derived from Prussian blue analogues, Sci. Bull. **62,** 358 (2017).

[11] J. W. McCargar and V. D. Neff, Thermodynamics of mixed-valence intercalation reactions: The electrochemical reduction of Prussian blue, J. Phys. Chem. **92,** 3598 (1988).

[12] M. Pasta, C. D. Wessells, Y. Cui, and F. La Mantia, A desalination battery, Nano Lett. **12,** 839 (2012).

[13] J. Lee, S. Kim, C. Kim, and J. Yoon, Hybrid capacitive deionization to enhance the desalination performance of capacitive techniques, Energy Environ. Sci. **7,** 3683 (2014).

[14] K. C. Smith and R. Dmello, Na-ion desalination (NID) enabled by Na-blocking membranes and symmetric Na-intercalation: Porous-electrode modeling, J. Electrochem. Soc. **163,** A530 (2016).

[15] T. Wu, G. Wang, S. Wang, F. Zhan, Y. Fu, H. Qiao, and J. Qiu, Highly stable hybrid capacitive deionization

with a MnO_2 anode and a positively charged cathode, Environ. Sci. Technol. Lett. **5**, 98 (2018).

[16] S. Shanbhag, Y. Bootwala, J. F. Whitacre, and M. S. Mauter, Ion transport and competition effects on $NaTi_2(PO_4)_3$ and $Na_4Mn_9O_{18}$ selective insertion electrode performance, Langmuir **33**, 12580 (2017).

[17] S. Kim, J. Lee, C. Kim, and J. Yoon, $Na_2FeP_2O_7$ as a novel material for hybrid capacitive deionization, Electrochim. Acta **203**, 265 (2016).

[18] A. M. Johnson and J. Newman, Desalting by means of porous electrodes, J. Electrochem. Soc. **118**, 510 (1971).

[19] T. R. Ferguson and M. Z. Bazant, Nonequilibrium thermodynamics of porous electrodes, J. Electrochem. Soc. **159**, A1967 (2012).

[20] M. Z. Bazant, K. Thornton, and A. Ajdari, Diffuse-charge dynamics in electrochemical systems, Phys. Rev. E **70**, 021506 (2004).

[21] P. M. Biesheuvel and M. Z. Bazant, Nonlinear dynamics of capacitive charging and desalination by porous electrodes, Phys. Rev. E **81**, 031502 (2010).

[22] P. M. Biesheuvel, Y. Fu, and M. Z. Bazant, Electrochemistry and capacitive charging of porous electrodes in asymmetric multicomponent electrolytes, Russ. J. Electrochem. **48**, 580 (2012).

[23] K. West, T. Jacobsen, and S. Atlung, Modeling of porous insertion electrodes with liquid electrolyte, J. Electrochem. Soc. **129**, 1480 (1982).

[24] B. E. Conway and E. Gileadi, Kinetic theory of pseudo-capacitance and electrode reactions at appreciable surface coverage, Trans. Faraday Soc. **58**, 2493 (1962).

[25] M. D. Levi and D. Aurbach, Frumkin intercalation isotherm—a tool for the description of lithium insertion into host materials: A review, Electrochim. Acta **45**, 167 (1999).

[26] W. Lai and F. Ciucci, Thermodynamics and kinetics of phase transformation in intercalation battery electrodes—phenomenological modeling, Electrochim. Acta **56**, 531 (2010).

[27] M. Z. Bazant, Theory of chemical kinetics and charge transfer based on nonequilibrium thermodynamics, Acc. Chem. Res. **46**, 1144 (2013).

[28] E. B. Nauman and D. Q. He, Nonlinear diffusion and phase separation, Chem. Eng. Sci. **56**, 1999 (2001).

[29] R. B. Smith and M. Z. Bazant, Multiphase porous electrode theory, J. Electrochem. Soc. **164**, E3291 (2017).

[30] T. R. Ferguson and M. Z. Bazant, Phase transformation dynamics in porous battery electrodes, Electrochim. Acta **146**, 89 (2014).

[31] Y. You, X.-L. Wu, Y.-X. Yin, and Y.-G. Guo, J. Mater. Chem. A **1**, 14061 (2013).

[32] P. Bai and M. Z. Bazant, Charge transfer kinetics at the solid–solid interface in porous electrodes, Nat. Commun. **5**, 3585 (2014).

[33] M. Doyle, T. F. Fuller, and J. Newman, Modeling of galvanostatic charge and discharge of the lithium/polymer/insertion cell, J. Electrochem. Soc. **140**, 1526 (1993).

[34] K. C. Smith, Theoretical evaluation of electrochemical cell architectures using cation intercalation electrodes for desalination, Electrochim. Acta **230**, 333 (2017).

[35] C. Erinmwingbovo, M. S. Palagonia, D. Brogioli, and F. L. Mantia, Intercalation into a Prussian blue derivative from solutions containing two species of cations, ChemPhysChem **18**, 917 (2017).

[36] A. A Sonin and R. F. Probstein, A hydrodynamic theory of desalination by electrodialysis, Desalination **5**, 293 (1968).

[37] T. M. Mubita, S. Porada, P. M. Biesheuvel, A. van der Wal, and J. E. Dykstra, Capacitive deionization with wire-shaped electrodes, Electrochim. Acta **270**, 165 (2018).

[38] J. E. Dykstra, K. J. Keesman, P. M. Biesheuvel, and A. van der Wal, Theory of pH changes in water desalination by capacitive deionization, Water Res. **119**, 178 (2017).

[39] M. Tedesco, H. V. M. Hamelers, and P. M. Biesheuvel, Nernst-Planck transport theory for (reverse) electrodialysis: II. Effect of water transport through ion-exchange membranes, J. Membr. Sci. **531**, 172 (2017).

[40] E. N. Guyes, A. N. Shocron, A. Simanovski, P. M. Biesheuvel, and M. E. Suss, A one-dimensional model for water desalination by flow-through electrode capacitive deionization, Desalination **415**, 8 (2017).

[41] S. A. Hawks, A. Ramachandran, P. G. Campbell, M. E. Suss, P. M. Biesheuvel, J. G. Santiago, and M. Stadermann, Performance metrics for the objective assessment of capacitive deionization systems, arXiv:1805.03247.